Euro. Jnl of Applied Mathematics (2016), *vol.* 27, *pp.* 667–685.
doi:10.1017/S0956792515000613

On the structure of generalized Poisson–Boltzmann equations

N. GAVISH[1] and K. PROMISLOW[2]

[1]*Department of Mathematics, Technion – Israel Institute of Technology, Haifa, Israel*
email: *ngavish@tx.technion.ac.il*
[2]*Department of Mathematics, Michigan State University, East Lansing, MI, USA*
email: *kpromisl@math.msu.edu*

(*Received 24 December 2014; revised 14 October 2015; accepted 16 October 2015; first published online 20 November 2015*)

In this work, we analyse a broad class of generalized Poisson–Boltzmann equations and reveal a common mathematical structure. In the limit of a wide electrode, we show that a broad class of generalized Poisson–Boltzmann equations admits a reduction that affords an explicit connection between the functional form of the corresponding free energy and the associated differential capacitance data. We exploit the relation to we show that differential capacitance curves generically undergo an inflection transition with increasing salt concentration, shifting from a local minimum near the point of zero charge for dilute solutions to a local maximum point near the point of zero charge for concentrated solutions. In addition, we develop a robust numerical method for solving generalized Poisson–Boltzmann equations which is easily applicable to the broad class of generalized Poisson–Boltzmann equations with very few code adjustments required for each model

Key words: Poisson-Boltzmann, differential capacitance, concentrated electrolyte solutions

1 Introduction

The contact between charged objects, such as a metal surface, macromolecule, or membrane, and an electrolyte solution results in the rearrangement of ionic distributions near the interface and formation of the so-called electrical double layer. The double layer has been extensively studied due to its importance within a wide number of areas including electrochemistry, biochemistry, physiology, and colloidal science.

The Poisson–Boltzmann (PB) theory is one of the most widely used analytical methods to describe double-layer structures. The PB theory is a continuum mean field-like approach assuming point-like ions immersed in a uniform dielectric medium and residing in thermodynamic equilibrium. The PB theory does not take into account the finite-size of the ions or their interaction among themselves and with the water molecules nearby them. As a result, the model is valid only when the charge on the interface is low and the electrolyte solution is dilute. Indeed, PB predictions deviate from experimental data even for mildly concentrated solutions or under moderate applied voltages, see [1] for a review.

Characterization of the double-layer structure in concentrated solutions or under high applied voltages is crucial to the understanding of many important systems such as fuel cells or ion channels [10,21]. The shortcomings of the PB model have led to the development of a large family of generalized PB equations which seek to describe the equilibrium ion profiles near a charged wall. These generalized PB models take into account the finite size of the ions [2,5,7–9,13,15,17–19], the dependence of the dielectric upon the electric field [4,6], or the dependence of the dielectric upon the local ionic concentration [3,12]. For a review of the different models, see [1] and references within. These models were in most cases validated by differential capacitance data, a measure of the overall charge imbalance in the system and one of the most important experimentally available characterizations of the electric double layer. The relation between model parameters and the differential capacitance data can be determined via the solution of the associated generalized PB equations. Accordingly, the study of each of the generalized PB models listed above and their prediction of the differential capacitance data was based on explicit solutions when such were available, or on a numerical study using methods customized specifically for the model considered. In many cases, the numerical and analytic study of these models focused on less-demanding symmetric cases.

In this work, we show that a broad class of generalized PB equations share a common structure that permits a considerable reduction in the limit of widely separated electrodes. In this limit, the generalized PB equations can be reduced to a dynamical system which is independent of the applied voltage, and possesses a single fixed point, corresponding to the bulk state far from the charged plates.

Utilizing dynamical systems techniques, we derive an explicit formula for the differential capacitance that directly relates the model parameters and its differential capacitance. This formula enables an analytic determination of the differential capacitance data without solving the associated generalized PB equations. Using the formula, we characterize the conditions under which differential capacitance undergoes an inflection transition from a local minimum point near the point of zero charge at dilute solutions to a local maximum point for concentrated solutions, and show that such a transition is generic.

We develop an efficient numerical scheme for solving generalized PB equations and for computing its differential capacitance. This method is based on backward shooting from the bulk state (saddle point) towards the electrode. Utilizing the common structure of generalized PB models, and specifically the fact that these models exhibit similar behaviour near the saddle point, makes this numerical scheme easily applicable to the broad class of generalized PB equations.

We demonstrate the numerical and analytical results by applying them to a generalized PB model which takes into account concentration-dependent dielectric [12]. To the best of our knowledge, the study of this model so far was restricted to the case of symmetric ion polarizability, probably to avoid numerical complications. The model's predictions are in fair agreement with experimental measurements in the regime of negative voltages, but not as good as the agreement for positive voltages. In [12], the authors state that *"to obtain similar agreement for positive voltage, it is necessary to use a different ion polarizability, as well as two different distances of closest approach, as the ions have different effective sizes in water."* Using the dynamical systems methods, we show that taking into account the different effective sizes of ions in water indeed yields a better agreement with the

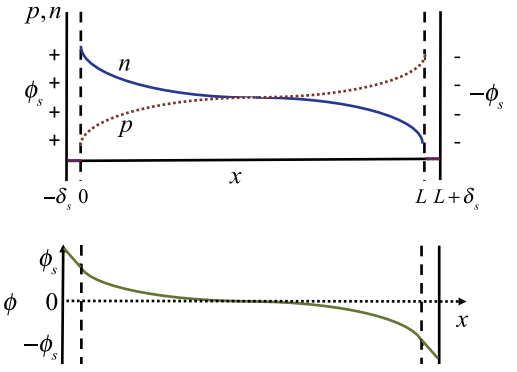

FIGURE 1. Illustration of the system of study. An electrolyte solution is bounded between two oppositely charged hard walls. Top graph presents the density profiles of the cations and of the anions, denoted by $p(x)$ and $n(x)$, respectively, where a Stern layer of width δ_s near each electrode is inaccessible to charge. The bottom graph presents the potential $\phi(x)$. Much of the focus of the paper will be in the case of infinite separation length $L \to \infty$.

theoretical and experimental results, while the data is less sensitive to ion polarizability. Moreover, at high ionic concentrations the model shows, in agreement with experiment data [11, 14], that the differential capacitance undergoes an inflection transition from a local minimum point near the point of zero charge at dilute solutions to a local maximum point for concentrated solutions.

The analytical and numerical tools presented herein allow a conceptual and numerical investigation of generalized PB equations that encompasses the impact of dielectric dependence on both electric field intensity and local ionic concentration.

Finally, the results of this paper fully address the forward problem: Given a generalized PB equation, what is its solution and what is the model's prediction for the differential capacitance data. This solution provides a solid and necessary basis for addressing the inverse problem which warrants further study: What are the classes of generalized PB models which give rise to prescribed differential capacitance data?

2 A class of generalized Poisson–Boltzmann models

We consider a 1:1 ionic solution bounded between two electrodes as shown in Figure 1. The walls are situated at $x = -\delta_s$ and $x = L + \delta_s$, where $\delta_s \geqslant 0$, with surface charge density such that the electric potential on the walls equals,

$$\phi(-\delta_s) = \phi_s, \quad \phi(L + \delta_s) = -\phi_s, \tag{2.1}$$

where the reference potential is taken to be zero voltage at the bulk. The ionic densities of the cations and of the anions are described by $p(x)$ and $n(x)$, respectively. A layer of width $\delta_s \geqslant 0$ near each electrode is inaccessible to charge, i.e.,

$$p(x) = n(x) = 0, \quad -\delta_s < x < 0, \quad L < x < L + \delta_s.$$

The average density of anions and cations is denoted by $\bar{c}$

$$\frac{1}{L}\int_0^L p(x)\,dx = \frac{1}{L}\int_0^L n(x)\,dx = \bar{c}.$$

The system is globally electroneutral. Therefore, when $\phi_s = 0$, the electric field vanishes $\phi'(x) = 0$ and

$$p = n \equiv \bar{c}, \quad \phi \equiv 0, \quad \phi'(x) \equiv 0. \tag{2.2}$$

The solvent is described as a dielectric medium with a general dielectric response $\epsilon(I, p, n)$ which depends locally on the electric field intensity $I := (\phi')^2$ and on the ionic concentrations. In subsequent sections, we will focus on the case of infinite separation length $L \to \infty$.

A Hamiltonian describing the system outside the Stern layers[1] is given by

$$\mathscr{A}(p,n,\phi) = \int_0^L k_B T \left[\underbrace{p\left(\ln\frac{p}{\bar{c}} - 1\right) + n\left(\ln\frac{n}{\bar{c}} - 1\right)}_{\text{entropy}} + \underbrace{f(p,n)}_{\text{non-ideality}} \right] + \underbrace{q(p-n)\phi - \frac{1}{2}\hat{\epsilon}(I,p,n)}_{\text{electrostatic}}\, dx, \tag{2.3}$$

where q is the unit of electrostatic charge, k_B is Boltzmann's constant, T is the temperature. The Hamiltonian consists of the standard entropic free energy together with a correction term $f(p,n)$ due to non-ideality caused by ion–ion interactions at concentrated solutions[2]. The last term $\hat{\epsilon}(I,p,n)$ is related to the (nonlinear) polarization of the material. The case

$$f(p,n) = 0, \quad \hat{\epsilon} = \epsilon_s I, \tag{2.4}$$

corresponds to the PB free energy which does not incorporate finite-size effects and treats the solvent as a uniform dielectric medium $\epsilon \equiv \epsilon_s$.

The double-layer structures we study are critical points of the action, $\mathscr{A}$; consequently, the generalized PB equations are derived by setting the variational derivatives of $\mathscr{A}$ with respect to p, n and ϕ equal to zero, see e.g. [8, Section 2]. Specifically, the variation of $\mathscr{A}$ with respect to ϕ yields a generalized Poisson equation

$$0 = \frac{\delta\mathscr{A}}{\delta\phi} = \frac{d}{dx}\left(\frac{\partial\hat{\epsilon}}{\partial I}\phi_x\right) + q(p-n) = 0, \qquad 0 < x < L, \tag{2.5a}$$

[1] A properly posed Hamiltonian should describe the full system without the need to separately handle the Stern layer regions, see, e.g., [13]. However, since Stern layers are introduced in many important models we have conformed to the common practice and consider a framework which can also treat Stern layers separately. We stress that all our results are valid in the absence of Stern layers, that is when $\delta_s = 0$.

[2] Our presentation is restricted to a non-ideality effect in entropy, for simplicity; extension to a non-ideality in enthalpy is straightforward.

in which the classic permittivity (dielectric) ϵ takes the form

$$\epsilon := \frac{\partial \hat{\epsilon}}{\partial I} = -2\frac{\delta \mathscr{A}}{\delta I}.$$

Following this observation, we will restrict ourselves to functions $\hat{\epsilon}$ that satisfy

$$\frac{\partial \hat{\epsilon}}{\partial I}(I, p, n) \geqslant \epsilon_0, \tag{2.5b}$$

where ϵ_0 is the vacuum permittivity. Within the Stern layer, the dielectric constant ϵ_s is assumed to be uniform, and therefore Poisson's equation reduces to $\epsilon\phi''(x) = 0$, whose solution is linear, and, subject to the boundary conditions (2.1), equals

$$\begin{aligned} &\phi(x) = \phi_s + (x + \delta_s)\phi'(0), && 0 \leqslant x \leqslant \delta_s, \\ &\phi(x) = -\phi_s + (x - L - \delta_s)\phi'(L), && L \leqslant x \leqslant L + \delta_s. \end{aligned}$$

Accordingly, (2.5*a*) is subject to the standard Stern boundary conditions

$$\phi(0) - d\phi'(0) = \phi_s, \qquad \phi(L) + d\phi'(L) = -\phi_s. \tag{2.5c}$$

Similarly, setting the variation of $\mathscr{A}$ with respect to p and n equal to zero and writing

$$h(I, p, n) := k_B T \left[p\left(\ln \frac{p}{\bar{c}} - 1\right) + n\left(\ln \frac{n}{\bar{c}} - 1\right) + f(p, n)\right] - \frac{1}{2}\hat{\epsilon}(I, p, n) \tag{2.5d}$$

gives rise to generalized Boltzmann equations for the charge density profiles in $0 < x < L$,

$$\begin{aligned} \lambda_p &= \frac{\delta \mathscr{A}}{\delta p} = h_p(I, p, n) + q\phi, \\ \lambda_n &= \frac{\delta \mathscr{A}}{\delta n} = h_n(I, p, n) - q\phi, \end{aligned} \tag{2.5e}$$

where λ_p and λ_n are the Lagrange multipliers associated with the conservation of mass

$$\frac{1}{L}\int_0^L p(x) - \bar{c}\, dx = 0 = \frac{1}{L}\int_0^L n(x) - \bar{c}\, dx. \tag{2.6}$$

For simplicity, the system (2.5) is non-dimensionalized by scaling

$$\tilde{\phi} = \frac{q}{k_B T}\phi, \quad \tilde{x} = \frac{x}{\lambda_D}, \quad \tilde{p} = \frac{p}{c^o}, \quad \tilde{n} = \frac{n}{c^o}, \quad \tilde{\bar{c}} = \frac{\bar{c}}{c^o}, \tag{2.7}$$

where λ_D is the Debye length

$$\lambda_D = \sqrt{\frac{k_B T \epsilon}{q^2 c^o}},$$

where c^o is an arbitrary reference density, see Remark 1 below. After the scaling, the bound (2.5*b*) takes the form

$$\hat{\epsilon}_I \geqslant 1. \tag{2.8}$$

Further, making the change of variables from ionic densities n and p to net charge density $\rho = n - p$ and total mass density $c = n + p$, defining

$$\tilde{h}(I, c, \rho) := h(I, p(c, \rho), n(c, \rho))$$

and using (2.2) to determining the Lagrange multipliers λ_p and λ_n yields the non-dimensional system (written after dropping the tildes)

$$\frac{d}{dx}\left[\frac{\partial \hat{\epsilon}}{\partial I}(c, \rho, I)\phi'(x)\right] = \rho, \tag{2.9a}$$

$$\begin{aligned} h_c(I, c, \rho) &= h_c(0, 2\bar{c}, 0), \\ h_\rho(I, c, \rho) &= \phi + h_\rho(0, 2\bar{c}, 0), \end{aligned} \tag{2.9b}$$

subject to boundary conditions

$$\phi(0) - \delta_s \phi'(0) = \phi_s, \qquad \phi(L) + \delta_s \phi'(L) = -\phi_s. \tag{2.9c}$$

Remark 1 *Note the explicit dependence of* (2.9) *in* $\bar{c}$. *Typically, this explicit dependence is eliminated by setting the reference density* c^o, *see* (2.7), *as the bulk density* $\bar{c}$. *We retain an arbitrary reference density,* c^o, *in order to preserve the central role played by the connection between the bulk density* $\bar{c}$ *and the Lagrange multipliers.*

3 Common structure of generalized Poisson–Boltzmann models

The system (2.9) is well defined only when equation (2.9*b*) uniquely defines $c(\phi, I, \bar{c})$ and $\rho(\phi, I, \bar{c})$. The following Lemma shows that this occurs if $h(I, c, \rho)$ is strictly convex in (c, ρ):

Lemma 1 *Equations* (2.9*b*) *uniquely define the functions* $c(\phi, I, \bar{c})$ *and* $\rho(\phi, I, \bar{c})$ *if* $h(I, c, \rho)$ *is a strictly convex function in* (c, ρ) *in the domain* $c > 0$.

Proof Let us rewrite equations (2.9*b*) as

$$\begin{aligned} F(c, \rho, \phi, I) &:= h_c(I, c, \rho) - h_c(0, 2\bar{c}, 0) = 0, \\ G(c, \rho, \phi, I) &:= h_\rho(I, c, \rho) - \phi - h_\rho(0, 2\bar{c}, 0) = 0. \end{aligned} \tag{3.1}$$

By the implicit function theorem, the system (3.1) locally defines $c(\phi, \bar{c}, I)$ and $\rho(\phi, \bar{c}, I)$ if the Jacobian

$$J := \frac{\partial(F, G)}{\partial(c, \rho)} = \text{Hessian}_{c,\rho}(h)$$

is invertible. The Jacobian equals the Hessian of h, which is a positive definite matrix since h is convex. Moreover, the local solution can be extended to a global one by a usual continuation argument when h is convex. □

In what follows, we will consider only the case where system (2.9) is well defined, i.e., the conditions of Lemma 1 hold. Lemma 1 implies that $\rho = \rho(\phi, I, \bar{c})$ and $c = c(\phi, I, \bar{c})$. The direct implication of this result is that generalized PB systems of the form (2.9) can be presented as autonomous dynamical systems. Indeed, the generalized Poisson's equation (2.9*a*) reduces to

$$\frac{\partial \hat{\epsilon}}{\partial I}\phi''(x) = \rho(\phi, I, \bar{c}) - \frac{d}{dx}\left(\frac{\partial \hat{\epsilon}}{\partial I}\right)\phi'(x).$$

Setting $E := \phi'(x)$, and applying the chain rule

$$\frac{d}{dx}\left(\frac{\partial \hat{\epsilon}}{\partial I}\right) = \frac{d\phi}{dx}\frac{d}{d\phi}\left(\frac{\partial \hat{\epsilon}}{\partial I}\right) = E\frac{d}{d\phi}\left(\frac{\partial \hat{\epsilon}}{\partial I}\right),$$

yields the autonomous dynamical system

$$\frac{d}{dx}\begin{bmatrix}\phi \\ E\end{bmatrix} = \begin{bmatrix}E \\ F(\phi, E; \bar{c}),\end{bmatrix}, \tag{3.2}$$

where $I = E^2$ and

$$F(\phi, E; \bar{c}) = \frac{\rho(\phi, I, \bar{c}) - I\frac{d}{d\phi}\hat{\epsilon}_I}{\hat{\epsilon}_I}.$$

Note that (2.8) ensures that the denominator of $F(\phi, E)$ is strictly positive.

The system has a fixed point at $(0, 0)$ which is a saddle point:

Lemma 2 *Under the conditions of Lemma 1 and for any* $\bar{c} > 0$ *and any* $L > 0$, *the dynamical system* (3.2) *has a single fixed point at* $(0, 0)$ *which is a saddle point.*

Proof Relations (2.2) imply that $\rho(0, 0; \bar{c}) = 0$. The bound (2.8) ensures that $F(0, 0) = 0$ and therefore the point $(0, 0)$ is a fixed point of (3.2).

The Jacobian of the system at $(0, 0)$ is

$$J = \left.\begin{bmatrix}0 & 1 \\ \rho_\phi/\hat{\epsilon}_I & \rho_E/\hat{\epsilon}_I\end{bmatrix}\right|_{(0,0)}.$$

The eigenvalues of J are given by

$$\lambda_\pm = \frac{\rho_E(0, 0) \pm \sqrt{\rho_E^2(0, 0) + 4\hat{\epsilon}_I(0, 0, 0)\rho_\phi(0, 0)}}{2\hat{\epsilon}_I(0, 0, 0)}, \tag{3.3}$$

with the corresponding eigenvectors

$$\mathbf{U}_\pm = \begin{bmatrix}\frac{1}{\lambda_\pm} \\ 1\end{bmatrix}. \tag{3.4}$$

We now show that $\rho_\phi > 0$ which implies, together with (2.8), that $\lambda_\pm$ have opposite signs and therefore that $(0, 0)$ is a saddle point. Indeed, differentiating (2.9*b*) with respect to ϕ

and substituting $E = 0$ yields

$$\text{Hessian}_{c,\rho}(h)|_{I=0} \begin{bmatrix} c_\phi \\ \rho_\phi \end{bmatrix} = \begin{bmatrix} 0 \\ 1 \end{bmatrix}.$$

By Lemma 1, Hessian$(h(0,\rho,c))$ is positive definite. Therefore, multiplying both sides by $[c_\phi, \rho_\phi]$ yields

$$[c_\phi, \rho_c]\ \text{Hessian}_{c,\rho}(h)|_{I=0} \begin{bmatrix} c_\phi \\ \rho_\phi \end{bmatrix} = [c_\phi, \rho_\phi] \begin{bmatrix} 0 \\ 1 \end{bmatrix} = \rho_\phi > 0. \tag{3.5}$$

Finally, we show that $(0,0)$ is the only fixed point of (3.2). Indeed, any fixed point of (3.2) must satisfy $E = 0$. Let us assume for contradiction that there exists an additional fixed point $(\phi^*, 0)$. Then,

$$F(\phi^*, 0) = \frac{\rho(\phi^*, 0)}{\hat{\epsilon}_I} = 0.$$

Thus, by (2.8), $\rho(\phi^*, 0) = 0$. However, relation (3.5) implies that $\rho_\phi > 0$, and we have shown that $\rho(0,0) = 0$, see (2.2). Thus, $\rho(\phi^*, 0) = 0$ if and only if $\phi^* = 0$. □

Lemma 2 shows that all generalized PB equations of the form (2.9) are described by dynamical systems which are locally homeomorphic. In particular, the saddle point structure is unperturbed under modifications to the action which preserve the convexity of h. From a physical point of view, the saddle point describes the bulk where $\phi \approx 0$ and $E \approx 0$. Therefore, Lemma 2 implies that generalizations of the PB model introduce terms which may give rise to significant changes near the electrodes and yield only quantitative, but not qualitative changes, in a neighbourhood of the bulk. We will exploit this property to analyse the large class of equations (2.9) and develop robust numerical methods for their solution.

A solution of (2.9) corresponds to a trajectory in the phase plane that starts from a point (ϕ_0, E_0) on the line

$$\phi_0 - \delta_s E_0 = \phi_s, \tag{3.6a}$$

see boundary conditions (2.9c), and reaches a point (ϕ_L, E_L) on the line

$$\phi_L + \delta_s E_L = \phi_s. \tag{3.6b}$$

These trajectories cannot pass throughout the saddle point $(0,0)$ as they reach the point (ϕ_L, E_L) at finite 'time' $(x = L)$. To illustrate this statement, we plot such trajectories for the PB system (2.4,2.9) with $\psi_s = 1$ and $\delta_s = 0.1$, in which case the dynamical system (3.2) reduces to

$$\begin{bmatrix} \phi \\ E \end{bmatrix}' = \begin{bmatrix} E \\ \sinh(\phi) \end{bmatrix}. \tag{3.7}$$

Specifically, in Figure 2 we plot the trajectories of (3.7) corresponding to the case $L = 2$ (dash–dotted) and $L = 3$ (dashes), and their corresponding solutions. We observe that these trajectories depend on L and δ_s. Indeed, this dependence can be found explicitly, by observing that the trajectories are the graphs of $(\phi, E(\phi))$, the Dirichlet-to-Neumann

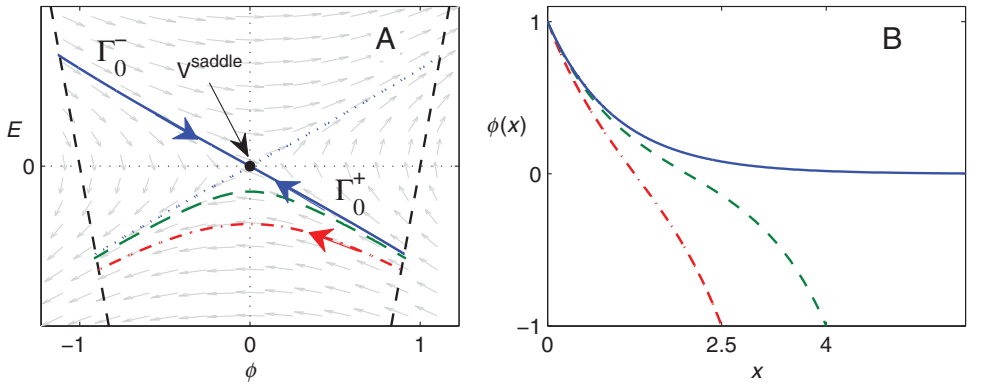

FIGURE 2. (A) Trajectories of the PB dynamical system, (3.7) with (2.4) and $\delta_s = 0.1$, corresponding to $\phi_s = 1$ and $L = 2$ (dash–dotted), $L = 3$ (dashes) and $L = \infty$ (solid). Also plotted is the trajectory Γ_0^- which corresponds to $L = \infty$ with $\phi_s = -1$, the lines $\phi - \delta_s E = \phi_s$ for $\phi_s = \pm 1$ (dashes), and the lines $\phi + \delta_s E = \phi_s$ for $\phi_s = \pm 1$ (dash–dotted) (B) Solutions $\phi(x)$ of (2.4,3.7) which correspond to the three trajectories in A with $\phi_s = 1$.

map, where $E = E(\phi)$ satisfies[3]

$$E'(\phi) = \frac{F(\phi, E)}{E(\phi)}, \tag{3.8}$$

subject to the boundary conditions (3.6), and the additional constraint that

$$x(\phi_L) = \int_{\phi_0}^{\phi_L} \frac{dx}{d\phi} d\phi = \int_{\phi_0}^{\phi_L} \frac{d\phi}{E(\phi)} = L.$$

3.1 The limit of infinite separation length

The limit $L \to \infty$ corresponds to infinite separation length between the two electrodes. By Lemma 2, the only fixed point of (3.2) is $(0, 0)$. Therefore, at $x \to \infty$, a trajectory can either go to the saddle point $(0, 0)$ or escape towards infinity $\lim_{x\to\infty} \phi(x) = \pm\infty$. The latter option is not possible since then the mass constraint boundary condition (2.6) would be violated. Therefore, the trajectory in the phase plane of (3.2) that corresponds to the solution of generalized PB equation in a one-electrode system is the Dirchlet-to-Neumann trajectory $\Gamma_0^{\pm}$ which is the unstable manifold of (3.2) at the saddle point. This trajectory satisfies the boundary conditions

$$\phi(0) - \delta_s \phi'(0) = \phi_s, \quad \phi(\infty) = 0, \quad E(\infty) = 0. \tag{3.9}$$

In addition, the mass constraints (2.6) reduce to

$$c(\infty) = 2\bar{c}, \qquad \rho(\infty) = 0.$$

[3] Equation (3.11) can be acquired by dividing (3.2) by $E := d\phi/dx$.

Accordingly, at the one-electrode setting, the system (2.9) reduces to the system

$$\frac{d}{dx}\left[\frac{\partial\hat{\epsilon}}{\partial I}(c,\rho,I)\phi'(x)\right]=\rho, \tag{3.10a}$$

$$\begin{aligned} h_c(c,\rho,I) &= h_c(2\bar{c},0,0),\\ h_\rho(c,\rho,I) &= \phi + h_\rho(2\bar{c},0,0), \end{aligned} \tag{3.10b}$$

subject to boundary conditions

$$\phi(0)-\delta_s\phi'(0)=\phi_s,\quad \phi(\infty)=0. \tag{3.10c}$$

A key observation of this study is that the Dirichlet-to-Neumann trajectories $\Gamma_0^{\pm}$ are independent of the value of ϕ_0 and of the value of δ_s. Rather, the values of ϕ_0 and δ_s merely determine the part of the trajectory which is present in the region $x\in(0,\infty)$, see, e.g., Figure 3. Indeed, the trajectories leaving the saddle point $(0,0)$ are the graphs of $(\phi,E(\phi))$ where $E=E(\phi)$ satisfies, see (3.8),[4]

$$E'(\phi)=\frac{F(\phi,E)}{E(\phi)},\qquad E(0)=0. \tag{3.11}$$

We conclude that the boundary condition of (2.9) at $x=0$ affects the dependence of $E=E(x)$ but not the form of the Dirichlet-to-Neumann map $E=E(\phi)$. From a physical point of view, the invariance of the Dirichlet-to-Neumann map implies that the electric potential and ionic density profiles will not change if one shifts the charged wall from $x=0$ to $x=x_0$ while changing the potential on the wall from $\phi(0)$ to $\phi(x_0)$. The invariance of E with respect to ϕ_0 holds only in the single planar-electrode setting. Indeed, as demonstrated in Figure 2, the critical point trajectory of (3.7) will depend significantly upon L, δ_s, and ϕ_0 when L is not large.

4 Differential capacitance

The total charge imbalance in the system equals (in non-dimensional form)

$$Q(\phi_s,\bar{c}) := \int_{-\delta_s}^{\infty}(p-n)\,dx.$$

The differential capacitance is defined as the change in surface charge q_s with respect to changes in the applied potential ϕ_s. Since the surface charge balances with the total charge imbalance, i.e., $q_s=-Q$, we obtain

$$C_D(\phi_s,\bar{c}) := \frac{\partial q_s}{\partial\phi_s}=-\frac{\partial Q}{\partial\phi_s}(\phi_s,\bar{c}).$$

Since charge imbalance occurs only in the electric double-layer region, differential capacitance data provides an important indirect measurement of double-layer structure.

[4] Note that this equation does not uniquely define $E(\phi)$ since the saddle point can be approached from two directions.

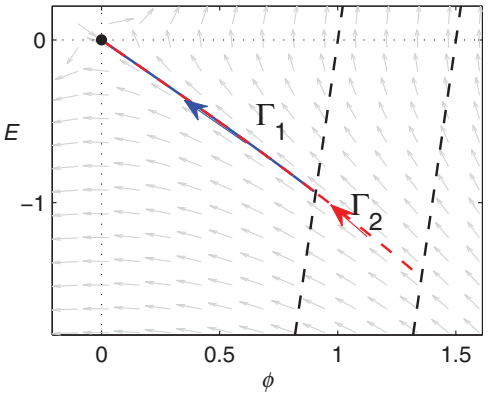

FIGURE 3. Trajectories Γ_0 of (3.7) with $d = 0.1$ corresponding to $\phi_0 = 1$ (solid) and $\phi_0 = 1.5$ (dashes). Also plotted are the lines $\phi = 1 + \delta_s E$ and $\phi = 1.5 + \delta_s E$ (dashes). Changing ϕ_0 merely modifies the part of the trajectory which is present in the region $x \in (0, \infty)$.

Traditionally, the differential capacitance data predicted by a generalized PB model is computed by solving the PB equations for the charge density profiles for each desired applied voltage, integrating the spatial dependence of the charge densities, and then differentiating the result with respect to applied voltage. The procedure is computationally inefficient and hides the underlying structure relating the generalized PB equation to the differential capacitance data.

The independence of the Dirichlet-to-Neumann map, $E(\phi, \bar{c})$ to ϕ_0, allows us to replace the boundary data ϕ_0 with the bulk value ϕ of the electric potential, and consequently derive an explicit formula for the differential capacitance. Taking into account that $\rho \equiv 0$ in the Stern layer, $-\delta_s < x < 0$, and substituting the LHS of Poisson's equation (2.5*a*) in the expression for the total charge imbalance yields

$$Q(\phi_s, \bar{c}) = -\int_{-\delta_s}^{\infty} \rho(x; \phi_s, \bar{c})\, dx = -\int_0^{\infty} \phi_{xx}(x; \phi_s, \bar{c})\, dx = \phi_x(x; \phi_s, \bar{c})|_{x=0} = E(\phi_0(\phi_s), \bar{c}). \tag{4.1}$$

Thus,

$$C_D(\phi_s, \bar{c}) = -\frac{d}{d\phi_s} E(\phi_0(\phi_s), \bar{c}) = -E'(\phi_0(\phi_s))\phi_0'(\phi_s).$$

This expression can be further resolved by differentiating both sides of relation (3.10*c*) by ϕ_s to obtain

$$\phi_0'(\phi_s) - \delta_s E'(\phi_0, \bar{c})\phi_0'(\phi_s) = 1.$$

Isolating $\phi_0'(\phi_s)$ and substituting the result into the expression for C_D yields

$$C_D(\phi_s, \bar{c}) = \frac{-E'(\phi_0)}{1 - \delta_s E'(\phi_0)}.$$

Finally, substituting ϕ for ϕ_0, and using (3.11), we find the expression

$$C_D(\phi_s, \bar{c}) = \frac{-F(\phi_0, E(\phi_0), \bar{c})}{E(\phi_0) - \delta_s F(\phi_0, E(\phi_0), \bar{c})}, \tag{4.2}$$

where (ϕ_0, E_0) is the intersection point of Γ_0 with the line $\phi - \delta_s E = \phi_s$. Note that the denominator of C_D is $E - \delta_s F \neq 0$ for $F \neq 0$ since $\text{sign}(F) = -\text{sign}(E)$.

The structure of equation (4.2) opens the way to a systematic analysis of the differential capacitance data, as it defines $C_D(\phi, \bar{c})$ in terms of $E(\phi)$ without recourse to the spatial profiles $p(x), n(x)$, or $\phi(x)$. The differential capacitance data can be extracted from the PB system (2.9) without solving the differential equations for each value of applied voltage ϕ_0, see Section 5. Many of the generalized PB models which take into account the finite size of the ions [2, 5, 7–9, 13, 15, 17–19] assume a uniform dielectric $\hat{\epsilon} = \epsilon_s I$ and do not incorporate a Stern layer. In this case, equation (4.2) reduces to the simple form

$$C_D(\phi_s, \bar{c}) = -\frac{\rho(\phi_s, \bar{c})}{E(\phi_s)}. \tag{4.3}$$

which relates the differential capacitance to the local ratio of the exposed charge and the electric field.

4.1 Inflection point

PB theory predicts that the differential capacitance has a pronounced minimum point near the point of zero charge. Experimental measurements show double-humped or dromedary-like differential profiles, see for example Figure 4, in which the local minima lies between two local maxima. These measurements, however, were conducted for dilute solutions. More recent works have shown that in concentrated solutions [8, 15, 16], differential capacitance has a maximum close to the potential of zero charge, rather than the familiar minimum. These results suggest that differential capacitance data undergoes an inflection transition from local minimum at dilute solutions to a local maximum for concentrated solutions.

Using relation (4.2), we can characterize the class of generalized PB models that predicts an inflection transition in the differential capacitance. For simplicity, we provide an example of the analysis in the absence of a Stern layer, and also in the symmetric case where $f_\rho \equiv 0$ and $\hat{\epsilon}_\rho \equiv 0$. The symmetry assures that $\phi = 0$ is a critical point of C_D. Indeed, by relations (4.2) and (3.10*b*)

$$C_D'(0) = 0,$$

and

$$C_D''(0) = \frac{1}{4}\sqrt{\frac{2\bar{c}}{\hat{\epsilon}_I}}\,\frac{1 - 4\left(f_{cc} - \frac{1}{2}\hat{\epsilon}_{cc} + \frac{3\hat{\epsilon}_{I,c}}{2\hat{\epsilon}_I}\right)\bar{c}}{1 + 2\left(f_{cc} - \frac{1}{2}\hat{\epsilon}_{cc}\right)\bar{c}} + \frac{1}{4}\sqrt{\frac{1}{2\bar{c}}}\left(40\bar{c} - \frac{16}{3}\right)\frac{\hat{\epsilon}_{I,\phi}^2}{\hat{\epsilon}_I^{3/2}} - \frac{9\sqrt{2\bar{c}}}{4}\frac{\hat{\epsilon}_{I,\phi\phi}}{\hat{\epsilon}_I^{3/2}}. \tag{4.4}$$

In the primitive case, $\hat{\epsilon}_I \equiv 1$, this expression reduces to

$$C_D''(0) = \frac{\sqrt{\bar{c}}}{2\sqrt{2}}\,\frac{1 - 4f_{cc}\bar{c}}{1 + 2f_{cc}\bar{c}}.$$

Therefore, at low concentrations and under the assumption that $f_{cc}(\bar{c})$ is bounded near $\bar{c} = 0$, the differential capacitance has a local minimum at the point of zero charge since we

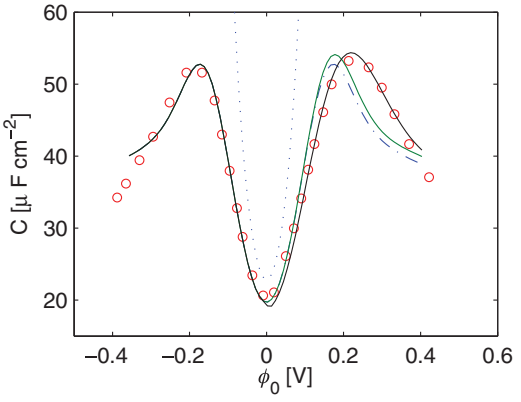

FIGURE 4. Experimentally measured differential capacitance curve, taken from [20, Figure 3] (red markers). The dotted blue curve is the prediction of the Gouy–Chapman model. The dash–dotted blue curve is the prediction by [12], equivalent to the system (3.10) subject to (6.1) with $\alpha_p = \alpha_n = -8$, and with a symmetric Stern layer of width $\delta_s = 0.48\,\text{nm}$. The solid green curve is the prediction of the same system with $\alpha_+ = -8$ and $\alpha_- = 3.2$, while the solid black curve results from an asymmetric Stern layer of width $\delta_s^+ = 0.48\,\text{nm}$ and $\delta_s^- = 0.6384\,\text{nm}$, and asymmetric excess polarization parameters $\alpha_+ = -8$ and $\alpha_- = 3.2$ (solid black).

have a local minimum point as $C_D''(0) \sim \sqrt{\bar{c}} > 0$. Conversely, if $f_{cc}(2\bar{c}, 0)\bar{c} \gg 1$ when $\bar{c} \gg 1$, then the critical point becomes a local maximum point and there is an inflection point for $\bar{c} = \bar{c}^*$ which solves

$$f_{cc}(2\bar{c}^*, 0) = \frac{1}{4\bar{c}^*}. \tag{4.5}$$

The Bikerman model [5], for example, corresponds to the choice of the excess free energy

$$f^{BK}(c) = \frac{1 - \nu c}{\nu} \log(1 - \nu c).$$

By substituting f^{BK} in (4.5) and solving the resulting equation for $\bar{c}^*$, we find that the Bikerman model gives rise to differential capacitance data that has an inflection point when $\bar{c}^* = \frac{1}{6\nu}$. This result can be directly verified by considering the Bikerman–Freise formula for the differential capacitance data [1]. In Section 6, we will use expression (4.4) to study inflection transition in a non-primitive model where $\hat{\epsilon} = \epsilon(c)I$.

5 Numerical methods

The generalized PB system is a non-linear boundary value problem which can be computed by an iterative process (to handle the non-linear terms) or by forward/backward shooting. We can utilize the dynamical system presentation to efficiently compute the solution of the generalized PB equation by adopting a backward shooting approach. As a basis for these computations, we assume that the functions $\rho(\phi, E)$ and $c(\phi, E)$ are known or are computed by solving (3.10*b*), and compute $E(\phi)$ by solving (3.11) using standard methods for computing an unstable manifold, e.g.,

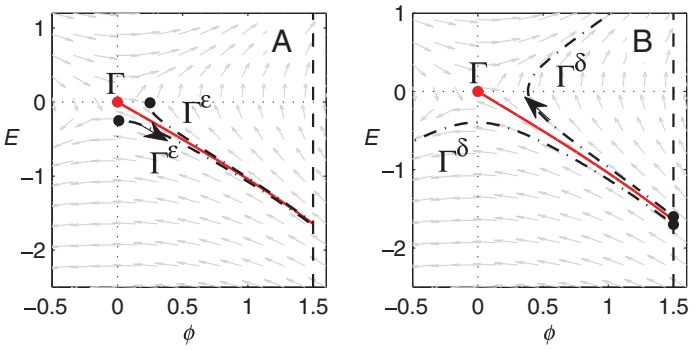

FIGURE 5. The trajectory Γ that corresponds to the solution of (3.10). Also plotted in (A) The trajectories Γ^{ϵ} which correspond to a backward solution with $E(L) = E_L - \varepsilon$. (B) The trajectories $\Gamma^{\pm\delta}$ which correspond to a forward solution with $E(0) = E_0 \pm \delta$.

Method 1 (Computation of $E(\phi)$) *Given* $\rho(\phi, E)$, $c(\phi, E)$[5] *and* $\hat{\epsilon}(\rho, c, I)$,

(1) *Set* $\phi_\delta = \text{sign}(\phi_0)\varepsilon$ *where* $0 < \varepsilon \ll 1$.

(2) *Solve the initial value problem* (3.11) *for* $\phi \in [\phi_\delta, \phi_0]$, *with the initial condition*

$$E(\phi = \phi_\delta) = \lambda_- \phi_\delta,$$

where λ_- *is given by* (3.3).

The method effectively computes the trajectory Γ_0 as it leaves the saddle point. The method is stable since Γ_0 is the unstable manifold of (3.2). Indeed, as illustrated in Figure 5(A) the distance between the trajectory Γ that corresponds to the solution of (3.10) and a trajectories Γ^{ϵ} which correspond to a backward solution with $E(\phi_\delta) = E - \varepsilon$ decreases with ϕ. Thus, we expect backward shooting to be stable for a broad class of generalized PB equations. In contrast, forward shooting would not be stable, since if the initial condition does not lie exactly on the trajectory Γ, then the trajectory corresponding to the forward solution would significantly deviate from Γ near the saddle point, see, e.g., Figure 5(B).

Traditionally, the differential capacitance data predicted by a generalized PB model is computed by solving the PB equations for the charge density profiles for each desired applied voltage, integrating the spatial dependence of the charge densities, and then differentiating the result with respect to applied voltage. The procedure is computationally inefficient and hides the underlying structure relating the generalized PB equation to the differential capacitance data. Using (4.2), the computation of the differential capacitance $C_D(\phi)$ becomes straightforward once $E(\phi)$ is known:

Method 2 (Computation of $C_D(\phi)$)

[5] The function $c(\phi, E)$ is introduced to the initial value problem (3.11) only via $\hat{\epsilon}(\rho, c, I)$. Thus, if $\hat{\epsilon} = \hat{\epsilon}(\rho, I)$, e.g., in the primitive case, there is no need to compute $c(\phi, E)$ in order to compute $E(\phi)$.

(1) *Compute* $E(\phi)$ *using Method 1.*

(2) *Compute* $\phi(0;\phi_s)$ *by solving the Algebraic equation*

$$\phi(0;\phi_s) - \delta_s E(\phi(0;\phi_s)) = \phi_s,$$

for each ϕ_s.

(3) *Compute* $C_D(\phi_s,\bar{c})$ *by direct substitution of* $E(\phi)$ *and* $\phi(0;\phi_s)$ *in* (4.2).

$$C_D(\phi_s,\bar{c}) = \frac{-F(\phi(0;\phi_s),E(\phi(0;\phi_s)),\bar{c})}{E(\phi(0;\phi_s)) - \delta_s F(\phi(0;\phi_s),E(\phi(0;\phi_s)),\bar{c})}.$$

In the absence of a Stern layer, the computation of C_D reduces to direct substitution of $E(\phi)$ in (4.3).

Backward shooting can also be used for computing the spatial profiles.

Method 3 (Computation of spatial profiles) *Given* ϕ_0, $\bar{c}$ *and* $\rho(\phi,E,\bar{c})$,

(1) *Set location of numerical boundary at* $x = L$.

(2) *Compute* $\phi(x)$ *by solving the system* (3.2) *for* $x < L$ *with the initial condition*

$$\phi(L) = \phi_L, \quad \phi_x(L) = E_L, \quad 0 \leqslant x \leqslant L,$$

where E_L *is the (possibly approximate) solution of*

$$\frac{\partial\hat{\epsilon}}{\partial I}(\phi_L,E_L^2)E_L = \int_0^{\phi_L} \frac{F(s;\bar{c})}{E(s;\bar{c})}ds, \tag{5.1}$$

and ϕ_L *is found by shooting so that the solution of (3.2) satisfies* $\phi(0) = \phi_0$.

(3) *If needed, compute* $E(x)$ *by direct substitution*

$$E(x) = E(\phi(x)).$$

(4) *Compute* $\rho(x,\bar{c})$ *and* $c(x,\bar{c})$ *by direct substitution*

$$\rho(x,\bar{c}) = \rho(\phi(x),\bar{c}), \qquad c(x,\bar{c}) = c(\phi(x),\bar{c}).$$

As in the methods above, Method 3 also involves solving an initial value problem and therefore can be computed by standard ODE solvers. Note, in addition, that it is possible to avoid solving the nonlinear integro-algebraic equation (5.1) for E_L, by obtaining an approximate solution for $\phi_L \ll 1$. Indeed, we have, for $0 < |\phi_L| \ll 1$,

$$\int_0^{\phi_L} \frac{\rho(s;\bar{c})}{E(s;\bar{c})}ds \approx \frac{\phi_L\rho(\phi_L)}{2E(\phi_L)}.$$

Thus, equation (5.1) reduces to

$$2\frac{\partial\hat{\epsilon}}{\partial I}(\phi_L, |E_L|^2)E_L^2 = \phi_L\rho(\phi_L),$$

and the solution is chosen such that $\text{sign}(E_L) = \text{sign}(\phi_L)$.

The method computes the trajectory Γ_0 as it leaves the saddle point, different from Method 1 only in the parametrization of the trajectory. As in Method 1 and as illustrated in Figure 5, we expect backward shooting to be stable for a broad class of generalized PB equations.

6 Example: Model with concentration-dependent dielectric

Recent work[6] of Hatlo *et al.* [12] considered the generalized PB system (3.10) with

$$\hat{\epsilon} = (\epsilon_w + \alpha_p p + \alpha_n n)I, \tag{6.1}$$

where typically $\alpha_p, \alpha_n < 0$. This choice of $\varepsilon(p, n)$ reflects the observation that typically ions reduce the dielectric of the solution in their vicinity. The case $\alpha_p = \alpha_n = 0$ reduces to the PB case. The work [12] considered only the symmetric case $\alpha_p = \alpha_n$, possibly to avoid numerical complications. The model was validated using differential capacitance data, and achieved a fair agreement with experimental predictions, primarily for negative voltages, see dash–dotted curve in Figure 4. In that paper, the authors stated that *"to obtain similar agreement for positive voltage, it is necessary to use a different ion polarizability, as well as two different distances of closest approach, as the ions have different effective sizes in water."* Our numerical study shows that taking into account these asymmetries, indeed, yields a better agreement between theoretical and experimental results, see solid black curve in Figure 4. Furthermore, we observe that the differential capacitance data is more sensitive to changes in Stern layer width than to ion polarizability, see solid green curve in Figure 4.

Further analysis of the differential capacitance curve in the symmetric case $\alpha := \alpha_p = \alpha_n$ can be conducted by studying relation (4.4) for $C_D''(0)$, for which it takes the simplified form

$$C_D''(0) = \frac{1}{4}\sqrt{\frac{2\bar{c}}{\hat{\epsilon}_I^3}}\left[\hat{\epsilon}_I - 6\alpha\bar{c} - 9\alpha c_{\phi\phi}\right].$$

As in Section 4.1, we find that the critical point in C_D changes from a local minimum to a local maximum as $\bar{c}$ increases through a critical value, all other effects held constant. This is depicted for the symmetric case in Figure 6(A) and for the antisymmetric case in Figure 6(B).

The study presented above did not require solving the generalized PB system (3.10) with (6.1). Using backward shooting, we can solve the generalized PB system for the spatial profiles, see Figure 7. In particular, Figure 7(C) presents the dielectric profile which reflects the balance of two effects: the attraction of the ions towards the oppositely

[6] Concurrently, [3] considered a generalized PB system with the same dielectric response function in a solution containing only negatively changed ions.

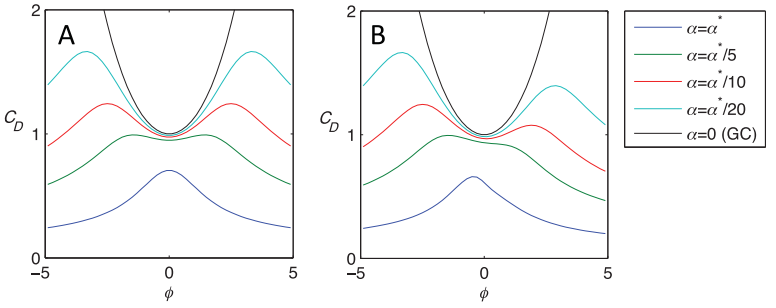

FIGURE 6. Differential capacitance curves computed for solutions of (2.9) with concentration dependent dielectric (6.1) for $\bar{c} = 1/2$ and for different values of α where (A) symmetric case $\alpha_p = \alpha_n = \alpha$. (B) asymmetric case, $\alpha_n = \alpha = 2\alpha_p$.

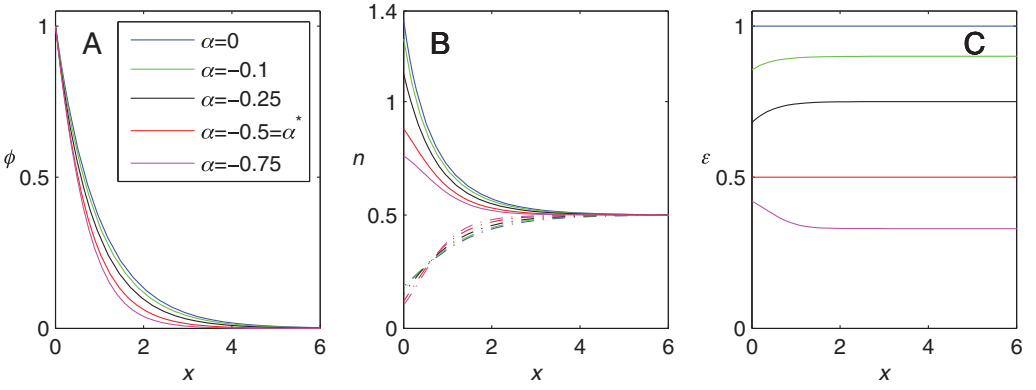

FIGURE 7. Solutions of (2.9) with concentration dependent dielectric (6.1) for $\bar{c} = 1/2$, $\phi_0 = 1$ and with different values of α. (A) Electric potential ϕ. (B) Concentration of negative ions n (solid curves) and positive ions p (dash–dotted curves). (C) Dielectric $\varepsilon(p, n)$.

charged plate and, for $\alpha < 0$, the repulsion of the ions from the plate due to their tendency to reduce the dielectric constant. For $\alpha < 0$ but sufficiently small in magnitude, the first effect dominates, and the dielectric decreases near the wall, while for sufficiently negative values of α the dielectric increases near the wall. At the border line case, the ionic profiles arrange so that the dielectric constant is spatially constant, this occurs for

$$\alpha_p = \alpha_n = \alpha^* = -\frac{1}{4}\frac{\varepsilon_w}{\bar{c}}.$$

This behaviour is depicted in Figure 7(C) where for $\alpha = \alpha^*$ we observe a uniform dielectric profile (compare also with [3, Figure 5]). Values of α near α^* are reasonable in physical systems, indeed setting $\varepsilon_w = 80$, we obtain that

$$\alpha^* = -\frac{20}{\bar{c}} \quad (M^{-1}).$$

Assuming that the model is valid for $\bar{c} < 2M$, we find that the range $M < \bar{c} < 2M$ corresponds to $-20 < \alpha^* < -10$. These values are comparable with $\alpha = -17$ for H^+

and $\alpha = -11$ for Li^+, $\alpha = -8$ for K^+, used in [12, Table 1]. Note that the experimental data considered in [12] was obtained for $\bar{c} = 0.01M$, for which $\alpha^* \ll \alpha$, far from the regime where monotonically decreasing or uniform dielectric profiles are observed.

7 Concluding remarks

In this work, we study a broad class of generalized PB equations. Surprisingly, we find that these equations can be reduced to autonomous dynamical systems, which all have a single saddle point corresponding to the bulk state far from the charged interface. Therefore, all generalized PB models share a common structure in the sense that no bifurcations occur due to the introduction of generalized terms.

A key result of this study is the derivation of an explicit formula for the differential capacitance data that directly relates the model parameters and its prediction for differential capacitance. This formula enables an analytic determination of the differential capacitance data without solving the associated generalized PB equations. Based on this result, we present analytical and numerical tools that allow a conceptual and numerical investigation of generalized PB equations, and in particular fully address the forward problem: Given a generalized PB equation, what is its solution and what is the model's prediction for the differential capacitance data. The solution of the forward problem provides a solid and necessary basis for addressing the inverse problem which warrants further study: What are the classes of generalized PB models which give rise to prescribed differential capacitance data?

Acknowledgement

The first author acknowledges support from the Technion VPR fund, EU Marie-Curie CIG grant 2018620, and Grand Energy Technion Program (GTEP) grant 1012217, while the second author acknowledges support from the NSF DMS grant 1109127 and 1409940.

References

[1] Bazant, M. Z., Sabri Kilic, M., Storey, B. D. & Ajdari, A. (2009) Towards an understanding of induced-charge electrokinetics at large applied voltages in concentrated solutions. *Adv. Colloid Interface Sci.* **152**(1–2), 48–88.

[2] Ben-Yaakov, D., Andelman, D., Harries, D. & Podgornik, R. (2009) Beyond standard Poisson–Boltzmann theory: Ion-specific interactions in aqueous solutions. *J. Phys.: Condens. Matter* **21**(42), 424106.

[3] Ben-Yaakov, D., Andelman, D. & Podgornik, R. (2011) Dielectric decrement as a source of ion-specific effects. *J. Chem. Phys.* **134**(7), 074705.

[4] Ben-Yaakov, D., Andelman, D., Podgornik, R. & Harries, D. (2011) Ion-specific hydration effects: Extending the Poisson-Boltzmann theory. *Curr. Opin. Colloid Interface Sci.* **16**(6), 542–550.

[5] Bikerman, J. J. (1942) Xxxix. structure and capacity of electrical double layer. *Phil. Mag.* **33**(220), 384–397.

[6] Booth, F. (1951) The dielectric constant of water and the saturation effect. *J. Chem. Phys.* **19**(4), 391–394.

[7] Boublík, T. (1970) Hard-sphere equation of state. *J. Chem. Phys.* **53**(1), 471–472.
[8] Di Caprio, D., Borkowska, Z. & Stafiej, J. (2003) Simple extension of the Gouy–Chapman theory including hard sphere effects: Diffuse layer contribution to the differential capacity curves for the electrode? electrolyte interface. *J. Electroanalytical Chem.* **540**(1), 17–23.
[9] di Caprio, D., Borkowska, Z. & Stafiej, J. (2004) Specific ionic interactions within a simple extension of the Gouy–Chapman theory including hard sphere effects. *J. Electroanal. Chem.* **572**(1), 51–59.
[10] Eisenberg, B. (2013) Interacting ions in biophysics: Real is not ideal. *Biophys. J.* **104**(9), 1849–1866.
[11] Fedorov M. V. & Kornyshev, A. A. (2014) Ionic liquids at electrified interfaces. *Chem. Rev.* **114**(5), 2978–3036.
[12] Hatlo, M. M., van Roij, R. & Lue, L. (2012) The electric double layer at high surface potentials: The influence of excess ion polarizability. *EPL (Europhys. Lett.)* **97**(2), 28010.
[13] Horng, T.-L., Lin, T.-C., Liu, C. & Eisenberg, B. S. (2012) PNP equations with steric effects: A model of ion flow through channels. *J. Phys. Chem. B* **116**(37), 11422–11441.
[14] Islam, M. M., Alam, M. T. & Ohsaka, T. (2008) Electrical double-layer structure in ionic liquids: A corroboration of the theoretical model by experimental results. *J. Phys. Chem. C* **112**(42), 16568–16574.
[15] Kilic, M., Bazant, M. Z. & Ajdari, A. (2007) Steric effects in the dynamics of electrolytes at large applied voltages. I. Double-layer charging. *Phys. Rev. E* **75**(2), 021502.
[16] Kornyshev, A. A. (2007) Double-Layer in ionic liquids: Paradigm change? *J. Phys. Chem. B* **111**(20), 5545–5557.
[17] López-García, J. J., Horno, J. & Grosse, C. (2011) Poisson–Boltzmann description of the electrical double layer including ion size effects. *Langmuir* **27**(23), 13970–13974.
[18] Mansoori, G. A., Carnahan, N. F., Starling, K. E. & Leland Jr, T. W. (1971) Equilibrium thermodynamic properties of the mixture of hard spheres. *J. Chem. Phys.* **54**(4), 1523–1525.
[19] Stern-Hamburg, H. O. (1924) Zur theorie c· der elektrolytischen doppelschicht, Z. Elektrochem. *S. f. Electrochemie* **30**, 508.
[20] Valette, G. (1981) Double layer on silver single crystal electrodes in contact with electrolytes having anions which are slightly specifically adsorbed: Part I. *J. Electroanal. Chem.* **122**, 285–297.
[21] Wei, G.-W., Zheng, Q., Chen, Z. & Xia, K. (2012) Variational multiscale models for charge transport. *SIAM Rev.* **54**(4), 699–754.